Available online at www.sciencedirect.com

ScienceDirect

journal homepage: www.elsevier.com/locate/he

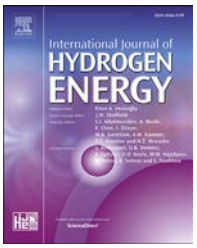

Effect of non-solvent from the phase inversion method on the morphology and performance of the anode supported microtubular solid oxide fuel cells

Cong Ren [a,b], *Yanxiang Zhang* [b,c], *Qi Xu* [a], *Tian Tian* [d], *Fanglin Chen* [b,*]

[a] *Department of Applied Chemistry, School of Advanced Materials and Nanotechnology, Xidian University, Xi'an 710071, PR China*

[b] *Department of Mechanical Engineering, University of South Carolina, Columbia, SC 29208, USA*

[c] *National Key Laboratory for Precision Hot Processing of Metals, MIIT Key Laboratory of Advanced Structure-Function Integrated Materials and Green Manufacturing Technology, School of Materials Science and Engineering, Harbin Institute of Technology, Harbin 150001, China*

[d] *School of Materials Science and Engineering, Shanghai Institute of Technology, Shanghai 201418, China*

HIGHLIGHTS

- Different non-solvent was used for SOFC fabrication via phase inversion method.
- Pore formation was explained by inter-diffusivity between solvent and non-solvent.
- Effect of anode microstructure on performance was analyzed by a polarization model.

ARTICLE INFO

Article history:
Received 2 November 2019
Received in revised form
13 December 2019
Accepted 16 December 2019
Available online xxx

Keywords:
Micro-tubular SOFCs
Anode support
Phase inversion method
Non-solvent
Inter-diffusivity

ABSTRACT

The microstructure of the anode in anode-supported solid oxide fuel cells has significant influence on the cell performance. In this work, microtubular Ni-yttria stabilized zircona ($Zr_{0.8}$ $Y_{0.2}O_2$, YSZ) anode support has been prepared by the phase inversion method. Different compositions of non-solvent have been used for the fabrication of the Ni-YSZ anode support, and the correlation between non-solvent composition and characteristics of the microstructure of the anode support has been investigated. The presence of ethanol or isopropanol in the non-solvent can inhibit the growth of the finger-like pores in the anode support. With the increase of the concentration of ethanol or isopropanol in the non-solvent, a thin dense layer can be observed on the top of the prepared tubular anode support. In addition, the mechanism of pore formation is explained based on the inter-diffusivity between the solvent and the non-solvent. The prepared microtubular solid oxide fuel cells (MT-SOFCs) have been tested, and the influence of the anode microstructure on the cell electrochemical performance is analyzed based on a polarization model.

© 2019 Hydrogen Energy Publications LLC. Published by Elsevier Ltd. All rights reserved.

* *Corresponding author.*
E-mail address: chenfa@cec.sc.edu (F. Chen).

https://doi.org/10.1016/j.ijhydene.2019.12.104

0360-3199/© 2019 Hydrogen Energy Publications LLC. Published by Elsevier Ltd. All rights reserved.

Please cite this article as: Ren C et al., Effect of non-solvent from the phase inversion method on the morphology and performance of the anode supported microtubular solid oxide fuel cells, International Journal of Hydrogen Energy, https://doi.org/10.1016/j.ijhydene.2019.12.104

Introduction

Solid oxide fuel cell (SOFC) is a promising energy conversion device due to its high energy conversion efficiency, environmental benign and excellent fuel flexibility [1–6]. Among various configurations of SOFCs, anode supported micro-tubular SOFCs (MT-SOFCs), which were initially proposed by Kendall et al. [7], exhibit several unique advantages such as higher volumetric density, faster start-up and higher tolerance of thermal cycling compared with other SOFC configurations. Therefore, many efforts have been devoted to developing anode supported MT-SOFCs [8]. It is well known that the anode microstructure plays a critical role in dictating the cell performance of anode-supported SOFCs by affecting mass transport as well as the electrochemical reactions in the anode [5,9]. Consequently, fabricating micro-tubular anode support with optimized microstructure has been an important endeavor for enhancing the cell performance of MT-SOFCs. So far, several methods have been adopted to control the anode microstructure [10–12]. Among them, SOFC anode fabricated by phase inversion process, a method that was initially developed by Loeb and Sourirajan for polymer membrane preparation [13], shows a unique asymmetrical microstructure [14], in which the layer with finger-like pores can function as desirable facile mass transport channels, and provide sufficient mechanical strength as well, while the layer with sponge-like pores close to the electrolyte side can enlarge the triple-phase boundaries (TPBs) and effectively enhance the electrochemical reactions in the anode. Based on this unique asymmetrical microstructured anode, MT-SOFCs with excellent electrochemical performance have been reported [15,16]. Moreover, Chen et al. investigated the correlation of this novel anode microstructure with the cell performance by establishing a numerical model [17].

To further optimize the anode microstructure in order to enhance the cell performance, the influence of fabrication parameters on microstructure has been extensively investigated such as slurry composition, polymer additive, inner solvent et al. [18–21]. In addition, employing a mixture of external coagulants is also one of these strategies to effectively tailor the microstructure. However, there is still discrepancy in the pore formation mechanism by using a mixture of coagulants among different studies. Jin et al. [22] correlated the microstructure with the non-solvent composition by the solubility criterion, which is based on the interaction between solvent and non-solvent. Deshmukh and Li [23] investigated the PVDF-DMAc system and indicated that the solvent and non-solvent interaction was not able to explain system with progressive reduction of precipitation rate, and they concluded that the mass transfer between solvent and non-solvent was the dominating factor affecting the pore formation. Currently, for the PESf-NMP system, which is the most used for MT-SOFC fabrication, its pore formation mechanism is still not explicitly unveiled.

In this work, phase inversion method using the PESf-NMP system with a mixture of non-solvent compositions is adopted to fabricate the NiO-YSZ anode supports. The pore formation mechanism is investigated and interpreted based on the inter-diffusivity between solvent and non-solvent. Furthermore, anode-supported MT-SOFCs with different microstructure are fabricated and tested, and the obtained current density-cell voltage (I–V) curves are analyzed based on a polarization model. Finally, the correlation between the anode microstructure and electrochemical performance of the anode-supported MT-SOFCs is also discussed.

Experimental

The microtubular anode supports were fabricated by the phase inversion method [15]. NiO and yttria stabilized zircona ($Zr_{0.8}Y_{0.2}O_2$, YSZ) powders were mixed in the weight ratio of 6:4 and ball milled using ethanol as milling media for more than 24 h, and then dried. The polymer binder polyethersulfone (PESf, Ameco Performance Radel A-300) was dissolved into the 1-methyl-2-pyrrolidone (NMP, HPLC grade, Sigma-Aldrich) solvent (1:7 in weight ratio, with a concentration of 0.147 g/mL). The NiO-YSZ mixed powders were dispersed into the polymer solution (1:1 in weight ratio), and then ball milled for 24 h with a rotation speed of 800r/min to achieve a stable casting slurry. Deionized water, water-ethanol mixture, and water-isopropanol mixture were used as the non-solvent in the external coagulant. At room temperature (25 °C), the micro-tubular anode supports with asymmetrical microstructure were prepared through a coating method, which has been described in detail previously [18], and the precipitation time of this experiment was 24 h. The prepared tubes were first heat-treated at 600 °C for 2 h to decompose the organic additives, and then heat-treated at 1200 °C for 2 h to obtain adequate mechanical strength for the electrolyte fabrication. YSZ thin film was deposited on the pre-sintered tubular samples using dip-coating method and then sintered at 1450 °C for 5 h to achieve the dense electrolyte. The $(La_{0.80}Sr_{0.20})_{0.95}MnO_{3-x}$ (LSM) powder was synthesized using the glycine nitrate process [24]. Glycine was added into the La, Sr, and Mn nitrate solution in a molar ratio of 2:1. The solution was then heated while stirring to evaporate water until self-combustion occurred. Subsequently, the precursor powder was calcined at 800 °C for 2 h to obtain the LSM powders. LSM-YSZ composite cathode was fabricated by a brush painting method and then sintered at 1100 °C for 2 h. The anode microstructure was examined by SEM (Zeiss Ultra plus FESEM). The prepared MT-SOFCs were tested at 750 °C using humidified H_2 (3 vol% H_2O) as fuel with the flow rate of 40 sccm for the anode and ambient air as the oxidant for the cathode. The electrochemical impedance spectra (EIS) and I–V curves were measured by multi-channel VersaSTAT (Princeton Applied Research). EIS was performed with an AC amplitude of 10 mV and frequency range from 100 KHz to 0.1 Hz.

Results and discussion

Microstructure of the NiO-YSZ anode support

The microstructure of samples fabricated with different non-solvent is shown in Fig. 1. Deionized water, 20 vol%, 50 vol %, 80 vol % ethanol-water mixture, 20 vol %, 50 vol %, and 80 vol % isopropanol-water mixture was used as the non-solvent for

Please cite this article as: Ren C et al., Effect of non-solvent from the phase inversion method on the morphology and performance of the anode supported microtubular solid oxide fuel cells, International Journal of Hydrogen Energy, https://doi.org/10.1016/j.ijhydene.2019.12.104

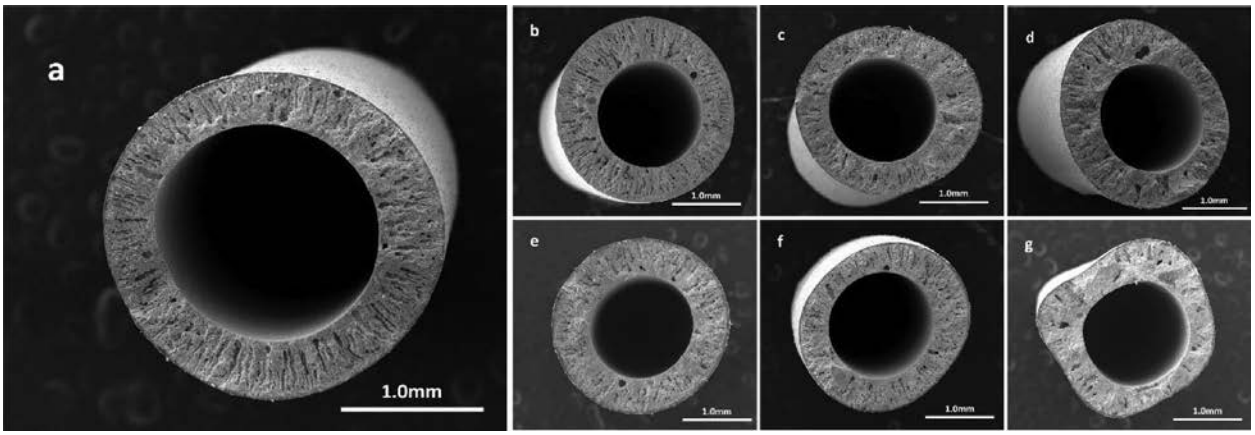

Fig. 1 – Microstructure of NiO-YSZ hollow fiber fabricated by non-solvent composed of (a) deionized water, (b) 20 vol% ethanol: 80 vol %water, (c) 50 vol % ethanol: 50 vol %water, (d) 80 vol % ethanol: 20 vol %water, (e) 20 vol % isopropanol: 80 vol %water, (f) 50 vol % isopropanol: 50 vol %water, (g) 80 vol % isopropanol: 20 vol %water.

precipitation. Fig. 1(a) shows the microstructure of pre-sintered sample prepared with deionized water as the non-solvent, where the typical asymmetric microstructure with two layers can be observed: a top layer (close to the exterior of the tube) with sponge-like pores and a sub-layer with larger finger-like pores. Fig. 1(b)-1(d) show the pre-sintered anode supports using 20 vol %, 50 vol %, and 80 vol % ethanol-water mixture as non-solvent, respectively. It can be observed that the length of the finger-like pores in the samples become shorter and the quantity of pores decreases as the increase of the ethanol content in the non-solvent, and a layer without finger-like pores forms close to the inner side of the tubes when using high ethanol content of the non-solvent. Moreover, the cross-section of the samples prepared with high ethanol content in the non-solvent shows that the wall thickness of the tube is not uniform, as shown in Fig. 1(d). The microstructure of the anode supports prepared using isopropanol-water mixture as the non-solvent with 20 vol %, 50 vol %, and 80 vol % isopropanol content can be seen from Fig. 1(e)-1(g). The inhabitation of finger-like pore formation and the generation of macrovoid-free layer close to the inner side of the tubes can also be observed as the isopropanol content increases. In Fig. 1(g), the cross-section of the samples fabricated with 80 vol % isopropanol content as the non-solvent shows that the wall thickness of the tube becomes irregular, and the tube seems to be obviously deformed, compared with the sample showing in Fig. 1(a).

The mechanism of the asymmetric microstructure formation can be explained based on the solvent and non-solvent interaction, when just considering the thermodynamic influence [23]. From this point of view, the solubility difference between the solvent and non-solvent is the main criterion for the microstructure predication. It has been reported that the solvent and non-solvent pair with larger solubility difference tends to start an instantaneous demixing and finally forms a porous geometry with finger-like pores [25]. As shown in Table 1, the increase of the volume ratio of ethanol or isopropanol in the non-solvent, the solubility difference decreases, which is calculated based on previous report [22]. According to the solubility criterion, the presence of ethanol or isopropanol in the non-solvent is expected to increase the probability to obtain finger-like geometry. However, as it can be observed in Fig. 1, finger-like pores are inhibited by using the non-solvent containing ethanol or isopropanol. Previously, Bottino *et al.* [26] indicated that in the PVDF system, thermodynamics had no significant influence on the final microstructure of the membrane and concluded that the inter-diffusivity of the solvent and non-solvent pair was the essential factor affecting the pore formation. Li and his co-authors [23] also studied the ethanol influence on the membrane microstructure in the PVDF system and indicated that in some systems mass transfer could be a major controlling factor in the pore formation process.

In the PESf-NMP system, the inter-diffusivity has been taken into consideration, as shown in Table 2; *D* values are

Table 1 – Differences of solubility parameters of NMP solvent and the different non-solvent.

Non-solvent	Solubility parameter $(\sqrt{\sum(\Delta\delta)^2})$ $MPa^{1/2}$
H_2O	35.4
20% ETOH	30.46
50%ETOH	23.7
80%ETOH	17.05
20%i-PrOH	30.07
50%i-PrOH	22.31
80%i-PrOH	15.16

Table 2 – Diffusion coefficients of NMP, ethanol and isopropanol.

Diffusion coefficient	$D \times 10^{-5}$ (cm^2/s)
$D_{NMP-water}$	0.821
$D_{NMP-ethanol}$	0.867
$D_{NMP-i-PrOH}$	0.412
$D_{water-NMP}$	1.461
$D_{ethanol-NMP}$	1.061
$D_{i-PrOH-NMP}$	0.947

Please cite this article as: Ren C et al., Effect of non-solvent from the phase inversion method on the morphology and performance of the anode supported microtubular solid oxide fuel cells, International Journal of Hydrogen Energy, https://doi.org/10.1016/j.ijhydene.2019.12.104

estimated by Tyn and Calus method [27] by the following equation:

$$D_{AB} = 8.93 \times 10^{-8} \frac{V_B^{0.267}}{V_A^{0.433}} \cdot \frac{T}{\eta_B} \left(\frac{\delta_B}{\delta_A}\right)^{0.15} \quad (1)$$

where D_{AB} is the diffusivity when A diffuses into B, V_i represents the molar volume at normal boiling point of solution i, η_i represents the viscosity of solution i, δ_i is the surface tension of solution i, and T is the temperature. It can be seen that.

$D_{NMP-water}$(0.821 × 10^{-5} (cm^2/s)) and $D_{NMP-ethanol}$ (0.867 × 10^{-5} (cm^2/s)) are comparatively close to each other and $D_{NMP-i-PrOH}$ (0.412 × 10^{-5} (cm^2/s)) shows almost half of the value of the $D_{NMP-water}$ and $D_{NMP-ethanol}$, indicating that the rate of NMP diffusing into isopropanol is much smaller than that diffusing into deionized water and ethanol. It can also be seen that $D_{water-NMP}$ (1.461 × 10^{-5} (cm^2/s)) is larger than $D_{ethanol-NMP}$ (1.061 × 10^{-5} (cm^2/s)) and $D_{i-PrOH-NMP}$ (0.947 × 10^{-5} (cm^2/s)). Therefore, water diffusing into the casting solution is faster than ethanol and isopropanol. After the precipitation is triggered, the low diffusion rate of the non-solvent (ethanol-water or isopropanol-water mixture) into the solvent (NMP) tends to reduce the rate of precipitation and finally inhibits the growth rate of the finger-like pores [23]. The microstructure results observed in Fig. 2 can also be well explained based on the inter-diffusivity influence. The microstructure of the anode supports prepared with deionized water only, or with 50 vol% ethanol is shown in Fig. 2(a) and (b), respectively. In Fig. 2(b), membranes with dense top layer can be observed, while in Fig. 2(a), membrane with a porous top layer is prepared by using only deionized water as the non-solvent. This result is also caused by different precipitation rates, and the slow diffusion rate of the non-solvent into the casting solution and the comparatively fast diffusion rate of the solvent out of the casting solution are tended to form a dense top layer according to the diffusion-controlled model [28]. Immediately after the dense top layer is formed, this layer will further hinder the diffusion of the solvent and non-solvent into each other. Non-solvent with high content of ethanol and isopropanol has smaller diffusion rate into the casting solution, and the diffusivity will also be reduced due to the formed dense layer, leading to the collapse of the mass flow between the casting solution and the coagulation bath. The hollow fiber has to deform to compensate the reduction of the amount of the non-solvent entered into the membrane, as shown in Fig. 1(g).

Performance of MT-SOFCs

Three types of MT-SOFCs are prepared based on the anode supports fabricated using deionized water only, 20 vol% ethanol-water mixture or 50 vol% ethanol-water mixture as the non-solvent, respectively, which show a gradual reduction of the finger-like pores in the anode microstructure. The cells are denoted as cell-a, cell-b and cell-c, respectively. Samples prepared with high ethanol content mixture and isopropanol mixture are not selected for cell fabrication due to the deformed noncircular cross-section of the anode supports. Fig. 3 shows the cross section of the tested tubular cells (cell-a, cell-b and cell-c), and the anode containing a functional layer and a gas diffusion layer with gradient finger-like pores can be observed, while the YSZ electrolyte is dense with a thickness of around 20 μm. Fig. 4 shows the electrochemical performance of cell-a, cell-b and cell-c tested at 750 °C. The open circuit voltages (OCV) of cell-a, cell-b and cell-c are 1.02 V, 1.03 V and 1.06 V, respectively. With the same testing condition, cell-a exhibits the best performance with the peak power density of 437 mW/cm^2, which is higher than 372 mW/cm^2 for cell-b and 293 mW/cm^2 for cell-c. Fig. 5 shows the EIS spectra of the different cells, revealing that cell-a has the smallest polarization resistance of 1.13 Ωcm^2 comparing with the others (1.54 and 2.53 Ωcm^2 for cell-b and cell-c, respectively). The different cell performances are expected to be attributed to the anode side because of the identical electrolyte and cathode materials are used for the cell fabrication. Previously, the enhancement of cell performance has been often ascribed to the optimal microstructure of the anode [15], and the anode support with longer finger-like pores is expected to be beneficial to the cell electrochemical performance because of the significantly decreased gas transport resistance in the anode.

Analysis of MT-SOFC performance

To further investigate the influence of the anode microstructure on the cell performance, a polarization model has been employed to analyze the *I*–*V* curves, showing the relationship of the current density (i) and the operating cell voltage (V_c):

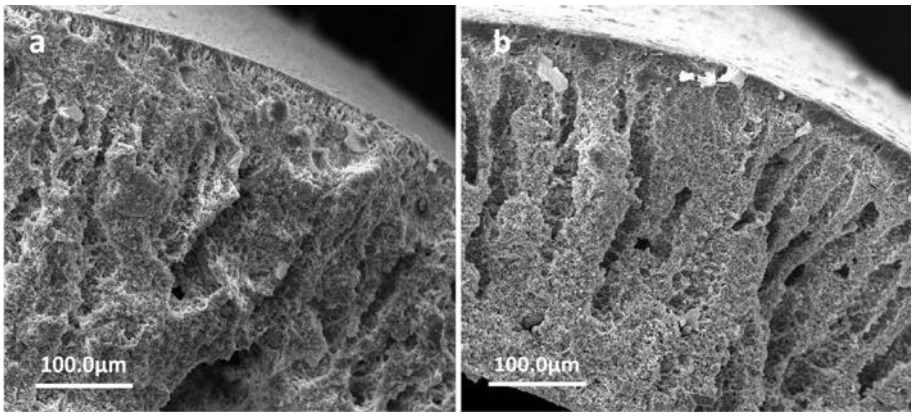

Fig. 2 – Microstructure of YSZ-NiO anode support fabricated by non-solvent composed of (a) deionized water, (b) 50 vol% ethanol: 50 vol% water.

Please cite this article as: Ren C et al., Effect of non-solvent from the phase inversion method on the morphology and performance of the anode supported microtubular solid oxide fuel cells, International Journal of Hydrogen Energy, https://doi.org/10.1016/j.ijhydene.2019.12.104

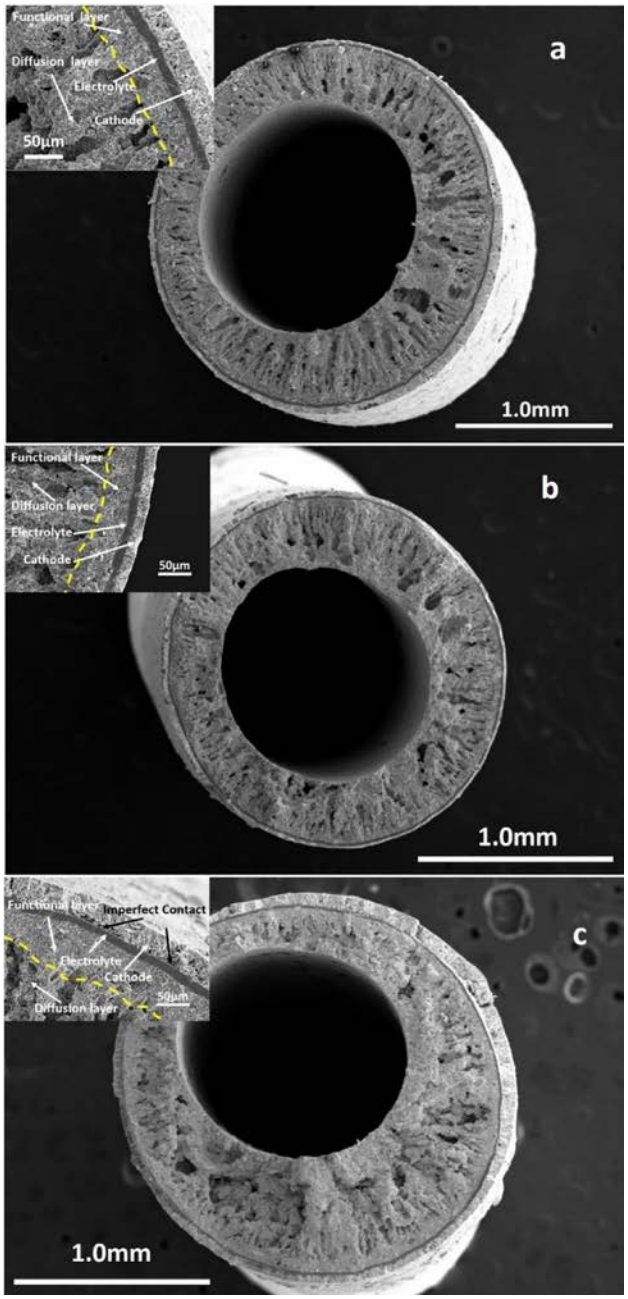

Fig. 3 – Cross-sectional fracture surface micrograph of cell-a (a), cell-b (b) and cell-c (c).

$$V_c = V_0 - iR_i - \eta_{act} - \eta_{a,conc} - \eta_{c,conc} - \eta_{leak} \quad (2)$$

where i is the current density (Acm^{-2}), R_i is the area specific ohmic resistance (Ωcm^2), V_o is the theoretical OCV (V) calculated by the Nernst equation, η_{act} is the activation polarization (V) resulting from both electrodes, $\eta_{a,conc}$ and $\eta_{c,conc}$ are the anodic and cathodic concentration polarization (V) respectively, and η_{leak} is the overpotential resulting from the imperfect sealing (V).

The V_o can be calculated by the Nernst equation. Since the YSZ electrolyte is dense, the discrepancy between the theoretical voltage and the measured value may be caused by the imperfect sealing, which is denoted as η_{leak} in Eq. (2). The main

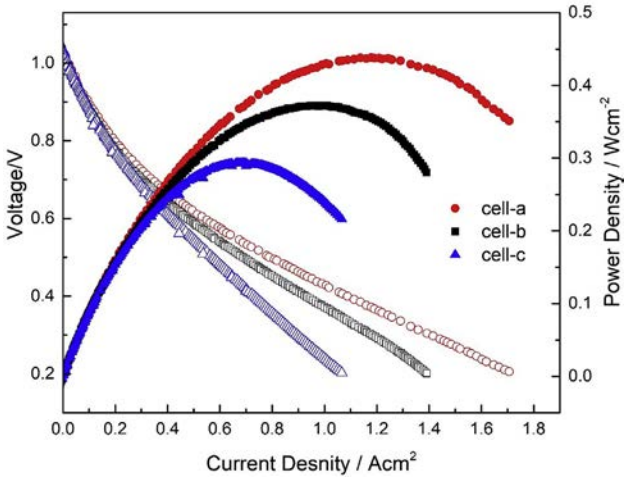

Fig. 4 – I–V curve and I–P curve of three types of cells with different anode structures, using humidified hydrogen (3 vol% H_2O) as fuel and ambient air as oxidant at 750 °C.

contribution of R_i results from the ohmic resistance of the electrolyte, as well as the ohmic resistance of the electrodes and the contact resistance from the interface between the different layers of the cell.

The activation polarization (η_{act}) arises from the charge transfer at the interface of the electrodes and electrolyte, and the relationship between activation polarization and current density can be described by the Butler-Volmer equation:

$$i = i_0 \exp\left(\frac{\alpha n \eta_{act} F}{RT}\right) - i_0 \exp\left(-\frac{(1-\alpha) n \eta_{act} F}{RT}\right) \quad (3)$$

where F is the Faraday constant, R is the universal gas constant, i_0 is the exchange current density, α is the transfer coefficient, n is the number of the electrons involved in the basic reaction of the SOFC operation. In this work, the electron transferred per reaction is 1 based on the electrochemical reactions occurring at cathode ($1/4O_2 + e^- \Leftrightarrow 1/2O^{2-}$) and anode ($1/2H_2 + 1/2O^{2-} \Leftrightarrow 1/2H_2O + e^-$) [29]. For the transfer coefficient, a symmetrical activation barrier has been proposed by Chan [29] and the transfer coefficient is taken as 0.5. Then, the equation can be expressed as

$$i = i_0 \exp\left(\frac{0.5 \eta_{act} F}{RT}\right) - i_0 \exp\left(-\frac{0.5 \eta_{act} F}{RT}\right) \quad (4)$$

To rewrite and solve the equation, the relationship

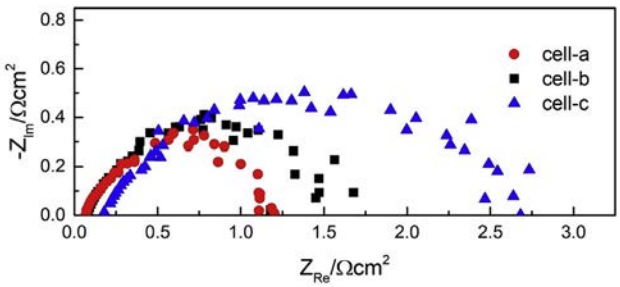

Fig. 5 – Electrochemical impedance spectra of cell-a, cell-b and cell-c at 750 °C under open circuit condition.

Please cite this article as: Ren C et al., Effect of non-solvent from the phase inversion method on the morphology and performance of the anode supported microtubular solid oxide fuel cells, International Journal of Hydrogen Energy, https://doi.org/10.1016/j.ijhydene.2019.12.104

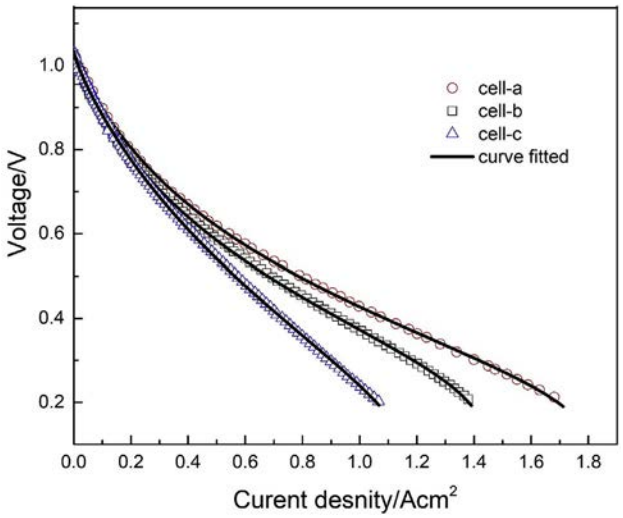

Fig. 6 – Experimental *I*–*V* curve of cell-a, cell-b and cell-c at 750 °C and corresponding polarization modeling results.

between the activation polarization and the current density can be described as [30].

$$\eta_{act} = \frac{2RT}{F}\ln\left\{\frac{1}{2}\left[\left(\frac{i}{i_0}\right) + \sqrt{\left(\frac{i}{i_0}\right)^2 + 4}\right]\right\} \quad (5)$$

where η_{act} represents the activation polarization from both the cathode and anode. The concentration polarization is derived from the mass transportation of gas through the porous electrodes. The cathodic concentration polarization can be expressed as [31]:

$$\eta_{c,conc} = -\frac{RT}{4F}\ln\left(\frac{p'_{o_{2(i)}}}{p^0_{o_2}}\right) = -\frac{RT}{4F}\ln\left(1 - \frac{i}{i_{cs}}\right) \quad (6)$$

where $P^0_{o_2}$ is the oxygen partial pressure outside of the cathode surface, and $P'_{o_{2(i)}}$ is the oxygen partial pressure at the interface of the cathode and electrolyte. i_{cs} is the cathode limit current density. When the current density reaches to the i_{cs}, the $P'_{o_{2(i)}}$ is zero. In this work, it is assumed that the cathode limit current density will not be affected when varying the microstructure of the anode.

For the anodic concentration polarization, it can be expressed as:

$$\eta_{a,conc} = -\frac{RT}{2F}\ln\left(\frac{p'_{H_{2(i)}}p^0_{H_2O}}{p^0_{H_2}p'_{H_2O(i)}}\right) = -\frac{RT}{2F}\ln\left(1 - \frac{i}{i_{as}}\right) + \frac{RT}{2F}\ln\left(1 + \frac{p^0_{H_2}i}{p^0_{H_2O}i_{as}}\right) \quad (7)$$

where $P'_{H_{2(i)}}$ is the hydrogen partial pressure at the interface of the anode and electrolyte, $P'_{H_2O_{(i)}}$ is the partial pressure of water vapor at the interface between the anode and electrolyte, $P^0_{H_2}$ and $P^0_{H_2O}$ are the hydrogen partial pressure and the partial pressure of water vapor outside the anode, respectively. i_{as} is the anodic limit current density that can be described as [31].

$$i_{as} = \frac{2FP^0_{H_2}D^{eff}_{H_2-H_2O}}{RTl_a} \quad (8)$$

where $D^{eff}_{H_2-H_2O}$ is the effective binary diffusivity of H_2 in H_2 and H_2O system. l_a is the thickness of the anode, which is ~500 μm.

In summary, the relationship of the current density (i) and the operating cell voltage (V_c) can be rewritten as:

$$V_c = V_0 - iR_i - \frac{2RT}{F}\ln\left\{\frac{1}{2}\left[\left(\frac{i}{i_0}\right) + \sqrt{\left(\frac{i}{i_0}\right)^2 + 4}\right]\right\} + \frac{RT}{2F}\ln\left(1 - \frac{i}{i_{as}}\right) - \frac{RT}{2F}\ln\left(1 + \frac{p^o_{H_2}i}{p^o_{H_2O}i_{as}}\right) + \frac{RT}{4F}\ln\left(1 - \frac{i}{i_{cs}}\right) - \eta_{leak} \quad (9)$$

The experimental data (*I*–*V* curves) have been fitted to Eq. (9) with five adjustable parameters, namely, R_i, i_{as}, i_{cs}, i_0 and η_{leak}. Fig. 6 compares the best fit to the experimental *I*–*V* data of different cells measured at 750 °C, and the parameters corresponding to the best fit are given in Table 3. The cathode limit current density (i_{cs}) of the cells is in the same order of magnitude. Fig. 7 shows the cathodic concentration polarizations calculated based equation (6) as a function of current density, and the concentration polarization loss from the cathode side shows small value even at a high current density. It has been reported that for the anode-supported cells with much thinner cathode, the cathode limit current density usually can not be precisely determined by the curve fitting [31]. Therefore, the gas diffusion performance of the cathode was not further analyzed in this work. The fitted exchange current density (i_0) ranges from 0.11 to 0.13 A/cm^2 due to the identical operating conditions and the same LSM-YSZ composite cathode employed. For the area specific ohmic resistance, the fitted results have good agreement with the measured ohmic resistance $R_{measure}$, which are extracted from the EIS spectra of the cells (Fig. 5), as listed in Table 3. The result shows that cell-c has a larger value of the area specific ohmic resistance than the other two cells. It has been known that the total ohmic resistance mainly coming from the electrolyte resistance and contact resistance between layers. Therefore, the increased ohmic loss of cell-c is likely due to the imperfect contact between the cathode and electrolyte, as shown in Fig. 3(c). The anodic limit current density (i_{as}) varies with the anode microstructure, where cell-a based on the anode support fabricated by using water as non-solvent shows the highest i_{as} among the tested cells. Based on this result, the concentration polarization values from the anode side can be calculated using equation (7) as a function of current density from Fig. 8. It shows that the anode concentration

Table 3 – Fitted parameters for the MT-SOFC.

MT-SOFC	$R_i/\Omega cm^2$	$R_{measure}/\Omega cm^2$	i_{as}/Acm^{-2}	i_{cs}/Acm^{-2}	i_0/Acm^{-2}	η_{leak}/V	$D^{eff}_{H_2-H_2O}/cm^2s^{-1}$
Cell-a	0.053	0.071	1.837	3.648×10^5	0.1195	0.1609	7.8×10^{-3}
Cell-b	0.068	0.092	1.461	3.638×10^5	0.1104	0.1605	6.2×10^{-3}
Cell-c	0.204	0.186	1.195	7.917×10^5	0.1338	0.1526	5.1×10^{-3}

Please cite this article as: Ren C et al., Effect of non-solvent from the phase inversion method on the morphology and performance of the anode supported microtubular solid oxide fuel cells, International Journal of Hydrogen Energy, https://doi.org/10.1016/j.ijhydene.2019.12.104

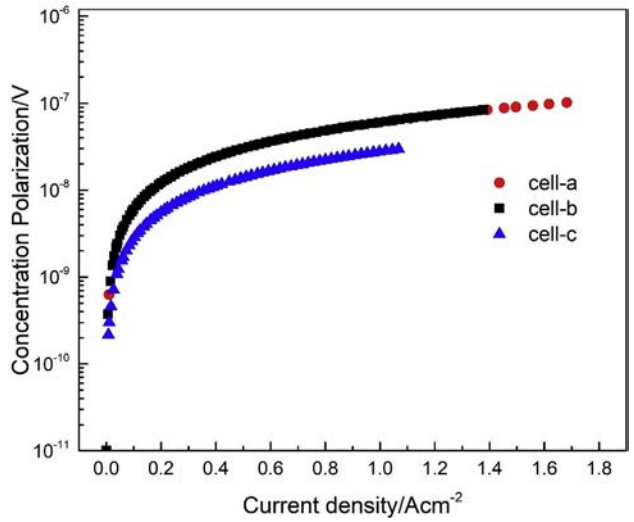

Fig. 7 – Calculated cathode concentration polarization of cell-a, cell-b and cell-c at 750 °C.

polarization values of cell-c and cell-b increase rapidly as the current density increases comparing with cell-a, indicating that the anode fabricated using water as non-solvent is beneficial to reducing the concentration polarization losses from the anode side. Moreover, the gas diffusion property of the anode microstructure can also be analyzed by estimating the effective binary diffusivity $D^{eff}_{H_2-H_2O}$ uisng Eq. (10), and the result is also listed in Table 3, showing that the effective binary diffusivity of the anode decreases from 7.8×10^{-3} to 5.1×10^{-3} cm^2s^{-1} corresponding from cell-a to cell-c. It has been reported that the effective binary diffusivity is significantly affected by the anode microstructure, and the relation can be described by the following equation [32].

$$D^{eff}_{H_2-H_2O} = D_{H_2-H_2O}\frac{p}{\tau} \quad (10)$$

where $D_{H_2-H_2O}$ is the gas diffusivity that does not account for the porous media, p and τ are the volume porosity and tortuosity factor of the anode microstructure, respectively. As a result of the same fuel composition and cell operating temperature, the $D_{H_2-H_2O}$ should be identical for every cell, according to the Chapman-Enskog equation [32]. Therefore, the value of the effective gas diffusivity is only affected by the parameters p and τ involving with the anode microstructure. The result suggests that anode support fabricated by using water as non-solvent with the largest $D^{eff}_{H_2-H_2O}$ is expected to be benefited from the long finger-like pores in the microstructure. Furthermore, the radial arranged finger-like pores can facilitate the fuel gas transportation, resulting in lower concentration polarization. It indicates that the anode with longer finger-like pores shows advantages over the anodes with other microstructure features, and water is a very promising non-solvent for the preparation of high-performance anode.

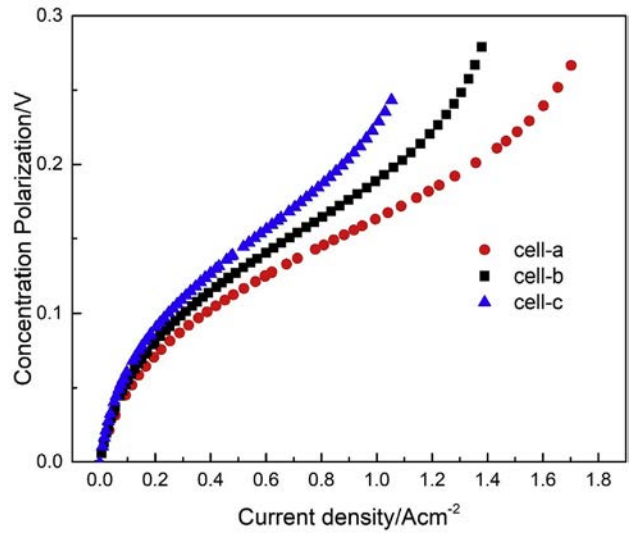

Fig. 8 – Calculated anode concentration polarization of cell-a, cell-b and cell-c at 750 °C.

Conclusion

The composition of the non-solvent coagulation is one of the key factors affecting the microstructure of the anode supports when selecting the NMP-PESf system. The formation of finger-like pores will be inhibited as the increase of the content of ethanol or isopropanol in non-solvent. The pore formation mechanism is interpreted based on the diffusion between the solvent and non-solvent. Three types of anode-supported MT-SOFCs are fabricated and tested corresponding to anodes with different finger-like pore length. Maximum power output of 437, 372 and 293 mW/cm^2 have been achieved for these three types of cells. The $I-V$ curves have been fitted by a polarization model, and MT-SOFCs based on the anode support fabricated by using water as non-solvent show the largest anodic limit current density, indicating that the longer finger-like pores in the anode can improve the gas transportation in the anode and decrease the anodic concentration polarization. This study reveals that the solvent and non-solvent pair with larger inter-diffusivity tends to promote the formation and growth of finger-like pores while MT-SOFCs with longer finger-like pores in the anode show better electrochemical performance. Our findings can provide insight to prepare high-performance anode-supported MT-SOFCs.

Acknowledgments

We gratefully acknowledge the financial support from National Natural Science Foundation of China (61605116, 51972208 and 51972213), the U.S. Department of Energy SOFC Core Technology Program (DE-FE0031670), and Fundamental Research Funds for the Central Universities (Grant NO. JB181402 and JBX171411).

REFERENCES

[1] Murray EP, Tsai T, Barnett SA. A direct-methane fuel cell with a ceria-based anode. Nature 1999;400:649–51.
[2] Kalinci Y, Dincer I. Analysis and performance assessment of NH_3 and H_2 fed SOFC with proton-conducting electrolyte. Int J Hydrogen Energy 2018;43:5795–807.
[3] Wang C, Lü Z, Su C, Li J, Cao Z, Zhu X, Wu Y, Li H. Effects of discharge mode and fuel treating temperature on the fuel

Please cite this article as: Ren C et al., Effect of non-solvent from the phase inversion method on the morphology and performance of the anode supported microtubular solid oxide fuel cells, International Journal of Hydrogen Energy, https://doi.org/10.1016/j.ijhydene.2019.12.104

utilization of direct carbon solid oxide fuel cell. Int J Hydrogen Energy 2019;44:1174–81.
[4] Lyu Z, Li H, Han M. Electrochemical properties and thermal neutral state of solid oxide fuel cells with direct internal reforming of methane. Int J Hydrogen Energy 2019;44:12151–62.
[5] Chen X, Lin J, Sun L, Liu T, Wu J, Sheng Z, Wang Y. Improvement of output performance of solid oxide fuel cell by optimizing the active anode functional layer. Electrochim Acta 2019;298:112–20.
[6] Wang Y, Lei X, Zhang Y, Chen F, Liu T. In-situ growth of metallic nanoparticles on perovskite parent as a hydrogen electrode for solid oxide cells. J Power Sources 2018;405:114–23.
[7] Kendall K, Palin M. A small solid oxide fuel cell demonstrator for microelectronic applications. J Power Sources 1998;71:268–70.
[8] Du Y, Sammes NM, Tomsett GA, Zhang D, Swan J, Bowden M. Extruded tubular strontium- and magnesium-doped lanthanum gallate, gadolinium-doped ceria, and yttria-stabilized zirconia electrolytes: mechanical and thermal properties. J Electrochem Soc 2003;150:A74–8.
[9] He W, Yoon KJ, Eriksen RS, Gopalan S, Basu SN, Pal UB. Out-of-cell measurements of H_2–H_2O effective binary diffusivity in the porous anode of solid oxide fuel cells (SOFCs). J Power Sources 2010;195:532–5.
[10] Suzuki T, Yamaguchi T, Fujishiro Y, Awano M. Fabrication and characterization of micro tubular SOFCs for operation in the intermediate temperature. J Power Sources 2006;160:73–7.
[11] Chen C, Liu M, Yang L, Liu M. Anode-supported micro-tubular SOFCs fabricated by a phase-inversion and dip-coating process. Int J Hydrogen Energy 2011;36:5604–10.
[12] Hedayat N, Panthi D, Du Y. Fabrication of anode-supported microtubular solid oxide fuel cells by sequential dip-coating and reduced sintering steps. Electrochim Acta 2017;258:694–702.
[13] Loeb S, Sourirajan S. Saline water conversion—II, advances in chemistry series, vol. 38. American Chemical Society; 1963. Ch. 9.
[14] Wu Z, Thursfield A, Metcalfe I, Li K. Effects of separation layer thickness on oxygen permeation and mechanical strength of DL-HFMR-ScSZ. J Membr Sci 2012;415:229–36.
[15] Othman MHD, Droushiotis N, Wu Z, Kelsall G, Li K. High-performance, anode-supported, microtubular SOFC prepared from single-step-fabricated, dual-layer hollow fibers. Adv Mater 2011;23:2480–3.
[16] Lu X, Li T, Bertei A, Cho JIS, Heenan TMM, Rabuni MF, Li K, Brett DJL, Shearing PR. The application of hierarchical structures in energy devices: new insights into the design of solid oxide fuel cells with enhanced mass transport. Energy Environ Sci 2018;11:2390–403.
[17] Chen B, Xu H, Ni M. Modelling of finger-like channelled anode support for SOFCs application. Sci Bull 2016;17:1324–32.
[18] Ren C, Liu T, Mao Y, Maturavongsadit P, Luckanagul JA, Wang Q, Chen F. Effect of casting slurry composition on anode support microstructure and cell performance of MT-SOFCs by phase inversion method. Electrochim Acta 2014;149:159–66.
[19] Liu T, Ren C, Fang S, Wang Y, Chen F. Microstructure tailoring of the nickel oxide-yttria-stabilized zirconia hollow fibers toward high-performance microtubular solid oxide fuel cells. ACS Appl Mater Interfaces 2014;6:18853–60.
[20] Ren C, Liu T, Maturavongsadit P, Luckanagul JA, Chen F. Effect of PEG additive on anode microstructure and cell performance of anode-supported MT-SOFCs fabricated by phase inversion method. J Power Sources 2015;279:774–80.
[21] Liu T, Ren C, Zhang Y, Wang Y, Lei L, Chen F. Solvent effects on the morphology and performance of the anode substrates for solid oxide fuel cells. J Power Sources 2017;363:304–10.
[22] Jin C, Yang C, Chen F. Effects on microstructure of NiO–YSZ anode support fabricated by phase-inversion method. J Membr Sci 2010;363:250–5.
[23] Deshmukh SP, Li K. Effect of ethanol composition in water coagulation bath on morphology of PVDF hollow fibre membranes. J Membr Sci 1998;150:75–85.
[24] Yang YJ, Wen TL, Tu H, Wang DQ, Yang J. Characteristics of lanthanum strontium chromite prepared by glycine nitrate process. Solid State Ion 2000;135:475–9.
[25] Smolders CA, Reuvers AJ, Boom RM, Wienk IM. Microstructures in phase-inversion membranes. Part 1. Formation of macrovoids. J Membr Sci 1992;73:259–75.
[26] Bottino A, Camera-Roda G, Capannelli G, Munari S. The formation of microporous polyvinylidene difluoride membranes by phase separation. J Membr Sci 1991;57:1–20.
[27] Reid RC, Prausnitz JM, Poling BE. The prosperities of gases and liquids. New York: Mc Craw-Hill; 1987. p. 601.
[28] Young TH, Chen LW. Pore formation mechanism of membranes from phase inversion process. Desalination 1995;103:233–47.
[29] Chan SH, Khor KA, Xia ZT. A complete polarization model of a solid oxide fuel cell and its sensitivity to the change of cell component thickness. J Power Sources 2001;93:130–40.
[30] Li PW, Chyu MK. Electrochemical and transport phenomena in solid oxide fuel cells. J Heat Transf 2005;127:1344–62.
[31] Kim JW, Virkar AV, Fung KZ, Mehta K, Singhal SC. Polarization effects in intermediate temperature, anode-supported solid oxide fuel cells. J Electrochem Soc 1999;146:69–78.
[32] Jiang Y, Virkar AV. Fuel composition and diluent effect on gas transport and performance of anode. J Electrochem Soc 2003;150:A942–51.

Nomenclature

D_{AB}: Binary diffusion coefficient of liquid species A and B, cm^2s^{-1}
V_i: Molar volume at normal boiling point of solution i, m^3mol^{-1}
η_i: Viscosity of solution i, kg $m^{-1}s^{-1}$
δ_i: Surface tension of solution i, Nm^{-1}
T: Temperature, K
V_c: Operating cell voltage, V
V_0: Theoretical cell voltage, V
η_{act}: Activation polarization, V
$\eta_{a,conc}$: Anode concentration polarization, V
$\eta_{c,conc}$: Cathode concentration polarization, V
η_{leak}: Overpotential resulting from the imperfect sealing,V
F: Faraday constant, $Cmol^{-1}$
α: Transfer coefficient
R: Universal gas constant, $Jmol^{-1}K^{-1}$
$P^0_{o_2}$: Oxygen partial pressure outside of the cathode, atm
$P'_{o_{2(i)}}$: Oxygen partial pressure at the interface of the cathode and electrolyte, atm
$P'_{H_{2(i)}}$: Hydrogen partial pressure at the interface of the anode and electrolyte, atm
$P'_{H_2O_{(i)}}$: Water vapor partial pressure at the interface between the anode and electrolyte, atm
$P^0_{H_2}$: Hydrogen partial pressure outside the anode, atm
$P^0_{H_2O}$: Water vapor partial pressure outside the anode, atm
l_a: Thickness of the anode, μm
i_{cs}: Cathode limit current density, Acm^{-2}
i_{as}: Anode limit current density, Acm^{-2}
i_0: Exchange current density, Acm^{-2}
$D_{H_2-H_2O}$: Binary diffusion coefficient of gaseous hydrogen and water vapor, cm^2s^{-1}
$D^{eff}_{H_2-H_2O}$: Effective binary diffusion coefficient of gaseous hydrogen and water vapor, cm^2s^{-1}
τ: Tortuosity factor
p: Porosity

Please cite this article as: Ren C et al., Effect of non-solvent from the phase inversion method on the morphology and performance of the anode supported microtubular solid oxide fuel cells, International Journal of Hydrogen Energy, https://doi.org/10.1016/j.ijhydene.2019.12.104